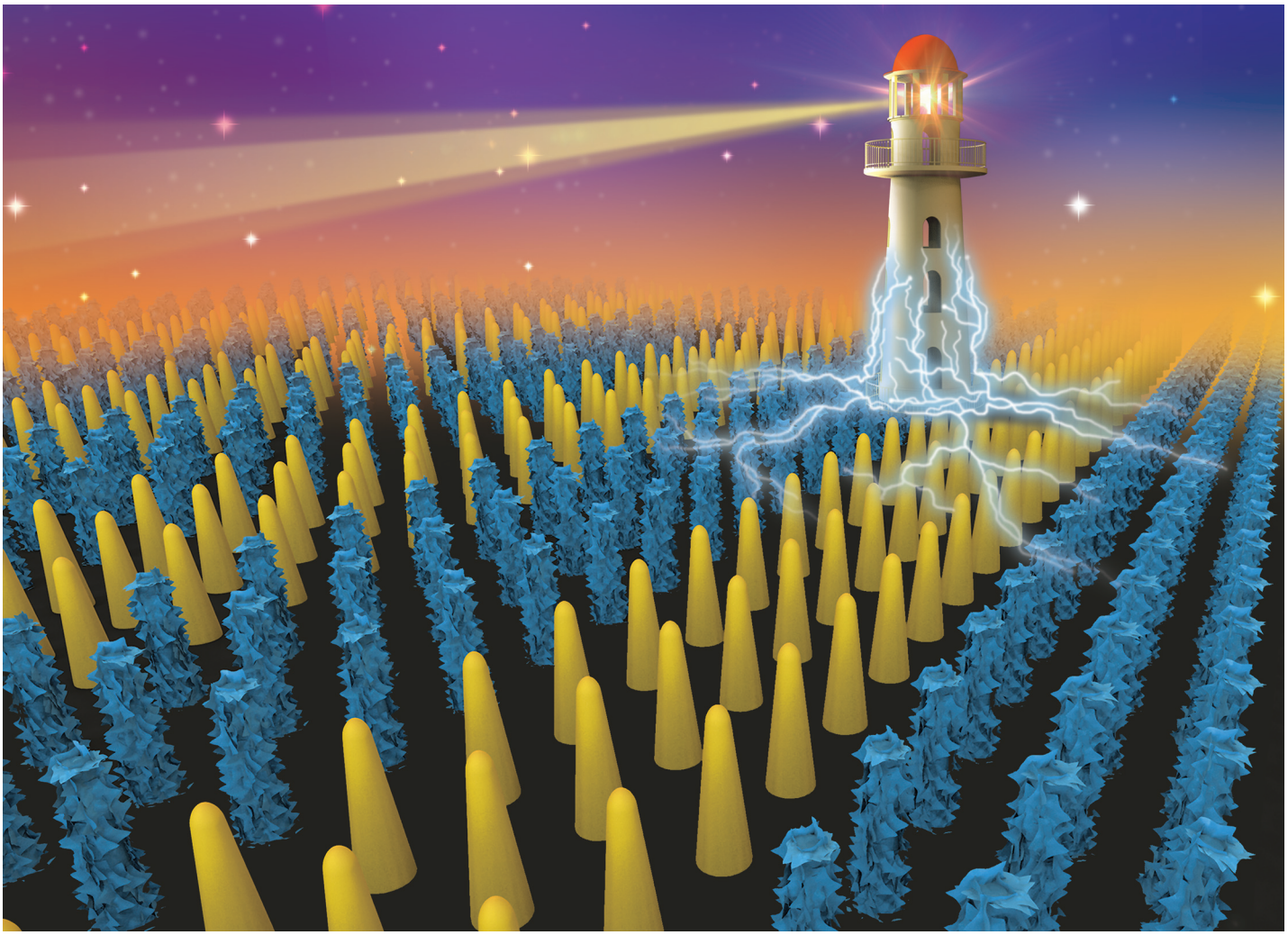

Showcasing research from the Beijing National Laboratory for Condensed Matter Physics, Institute of Physics, Chinese Academy of Sciences, Beijing, China.

Side-by-side observation of the interfacial improvement of vertical graphene-coated silicon nanocone anodes for lithium-ion batteries by patterning technology

A vertical graphene–silicon nanocone composite anode for lithium-ion batteries is specially designed. The coating patterning technology is innovatively employed for side-by-side comparison between the graphene-coated area and the uncoated area. The work clearly indicates the improved electrochemical performance, solid electrolyte interphase formation, and structural stability attributed to the vertical graphene coating. The as-proposed patterning technology is of significant guidance like a lighthouse for comparative research on coating materials for silicon anodes.

As featured in:

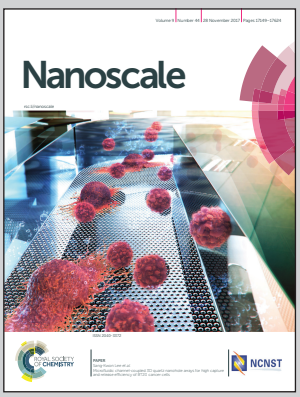

See Junjie Li, Changzhi Gu, Hong Li *et al.*, *Nanoscale*, 2017, **9**, 17241.

ROYAL SOCIETY OF CHEMISTRY

rsc.li/nanoscale

Registered charity number: 207890

Nanoscale

PAPER

View Article Online
View Journal | View Issue

Cite this: *Nanoscale*, 2017, **9**, 17241

Side-by-side observation of the interfacial improvement of vertical graphene-coated silicon nanocone anodes for lithium-ion batteries by patterning technology

Chao Wang,[a,b] Fei Luo,[c] Hao Lu,[a] Bonan Liu,[a] Geng Chu,[a] Baogang Quan,[a] Junjie Li,*[a,b] Changzhi Gu,*[a,b,d] Hong Li*[a] and Liquan Chen[a]

We report that vertical graphene coating can greatly improve the electrochemical performance and the interfacial stability of silicon nanocone (SNC) anodes for lithium-ion batteries. The coating patterning technology is innovatively employed for side-by-side demonstration of the exclusive influences of graphene coating on the solid–electrolyte interphase (SEI) formation and the structural stability of the SNC electrode. The silicon nanocone–graphene (SNC-G) electrode achieves a longer cycle life (1715 cycles), higher Coulombic efficiency (average 98.2%), better rate capability, and lower electrode polarization than the SNC electrode. The patterning of the graphene coating provides a much direct and convincing morphological comparison between the SNC-G structure and the SNC structure, showing clearly that the SNC-G area maintains a thin SEI layer and stable nanostructure after cycling, while the SNC area is gradually damaged and covered with a thick SEI layer after 100 cycles. Our results clearly indicate the improved electrochemical performance and interfacial stability attributed to the vertical graphene coating, and the as-proposed patterning technology also paves a new way for comparative research on coating materials for lithium-ion batteries.

Received 7th June 2017,
Accepted 25th July 2017

DOI: 10.1039/c7nr04041e

rsc.li/nanoscale

Introduction

Lithium-ion batteries play an important role in electronic devices in both the military field and the civilian field because of their relatively high energy density and long cycle life.[1,2] To further improve the energy density for higher demands, new electrode materials such as Si, Ge, Sn, and Sb have been extensively studied, in which silicon is one of the most promising anodes for next generation lithium-ion batteries.[3,4] Silicon has a high specific capacity by forming $Li_{15}Si_4$ (3580 mA h g^{-1}) at room temperature, which is ten times higher than conventional graphite anodes.[5] Meanwhile, silicon also has the advantages of harmlessness, abundant reserve, and mature production technology.[6] However, the application of silicon anodes is still hindered by two major disadvantages of tremendous volume change (~300%) and continuous solid–electrolyte interphase (SEI) formation,[7] which would cause structural pulverization and electrolyte consumption, leading to poor cycling performance and low Coulombic efficiency of the batteries.[8]

Recent studies have shown that nanostructured silicon such as nanowires,[9,10] nanotubes,[11,12] and nanoparticles[13,14] can avoid fracture and offer free space to accommodate the volume expansion, thus improving the specific capacity and cycle life of the batteries.[15] Coating materials such as carbon,[16] graphene,[17,18] metals,[19] and metal oxides[20] have been applied to silicon anodes to improve the electrochemical performance, in which graphene has attracted lots of attention due to its unique physical and chemical properties. Graphene has remarkable mechanical strength, excellent chemical stability, and high electrical conductivity,[21,22] thus providing great advantages of accommodating the volume expansion, suppressing the SEI formation, and enhancing the electrical conductivity of the silicon anodes.[23,24]

However, few research studies have really shown the exclusive influences of graphene coating on the SEI formation, structural stability, and electrochemical performance of silicon anodes for the reason that most nanostructured silicon has an irregular shape for distinct SEM observation and the influence of additives and binders is difficult to eliminate. In particular,

[a]*Beijing National Laboratory for Condensed Matter Physics, Institute of Physics, Chinese Academy of Sciences, Beijing 100190, P. R. China. E-mail: jjli@iphy.ac.cn, czgu@iphy.ac.cn, hli@iphy.ac.cn*
[b]*School of Physical Sciences, CAS Key Laboratory of Vacuum Physics, University of Chinese Academy of Sciences, Beijing 100190, P. R. China*
[c]*Department of Chemistry, Tsinghua University, Beijing 100084, P. R. China*
[d]*Collaborative Innovation Center of Quantum Matter, Beijing 100190, P. R. China*

a side-by-side comparison between the coated area and the uncoated area has not been reported in the literature before, and the direct comparison is much convincing for deeply understanding the enhanced electrochemical performance attributed to graphene coating.

Here, the silicon nanocone (SNC) model anode and the coating patterning technology have been combined for the first time to demonstrate the significant influences of graphene coating on the electrochemical performance, SEI formation, and structural stability of the silicon anodes. The SNC electrode is fabricated by using an inductively coupled plasma reactive ion etching (ICP) system. The nanocone structure has the advantages of sufficient intercone space, pure component, and regular morphology, which are very helpful for observing SEI formation and eliminating the influence of additives. The vertical graphene is coated on the SNC electrode using the hot-filament chemical vapor deposition (HFCVD) method. The three-dimensional petaloid structure is more beneficial for accommodating the strain of volume change during cycling, thus enhancing the mechanical integrity and improving the interfacial properties.[25] The three-dimensional conductive network can also facilitate lithium transportation and promote the electronic conductivity of the SNC electrode.[26] Moreover, the ultraviolet lithography (UVL) and reactive ion etching (RIE) technologies are applied to the silicon nanocone–graphene (SNC-G) electrode to obtain the silicon nanocone–patterned graphene (SNC-PG) electrode, which enables the SNC structure and SNC-G structure to be tested on the same electrode, thus making the comparison between these two structures more direct and convincing. The SNC-G electrode shows promising electrochemical performance, and the coating patterning technology also provides a platform for side-by-side comparison to investigate the coating-enhanced performance and the related mechanism of the silicon anodes in lithium-ion batteries. The fabrication process of the SNC, SNC-G, and SNC-PG electrodes is schematically shown in Fig. 1.

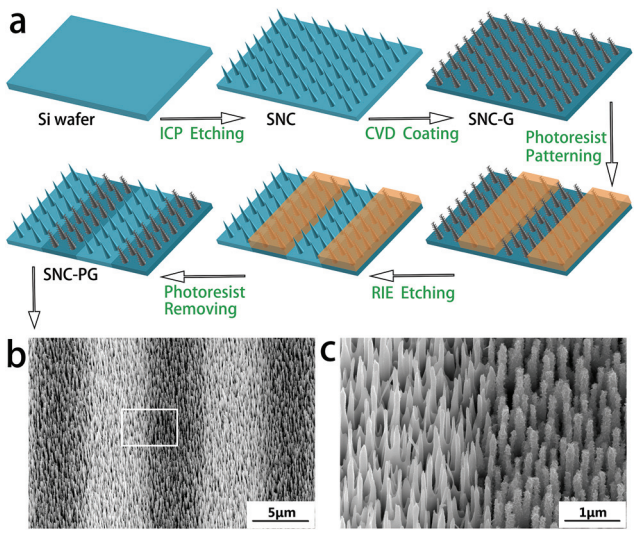

Fig. 1 (a) Schematic diagram of the fabrication process of the SNC, SNC-G, and SNC-PG electrodes. (b) A SEM image of the SNC-PG electrode corresponding to the schematic diagram. (c) A higher-magnification SEM image for the SNC-PG electrode from the white box in (b).

Experimental

Material preparation

The SNC electrode was obtained by directly etching the silicon wafer using an inductively coupled plasma reactive ion etching system (ICP, Oxford PlasmaPro 100 Cobra). The etching gases were oxygen and sulfur hexafluoride. By changing the etching power, gas flow ratio, temperature, and gas pressure, the aspect ratios of the SNCs could be modulated. The vertical graphene was grown on the SNCs by the hot-filament chemical vapor deposition (HFCVD) method. The reactant gases were methane, hydrogen, and argon with a ratio of 1 : 5 : 45 and a sustaining gas pressure of 2.5 kPa. The reaction was controlled at 1000 °C for 3 minutes. A bias voltage was added between the filament and the substrate to facilitate the growth of graphene. The ultraviolet lithography (UVL) and reactive ion etching (RIE) technologies were applied to the SNC-G electrode to obtain patterned graphene coating. A 1 μm thick photoresist (AZ6130) layer was coated on the SNC-G electrode, and then the electrode was exposed in the UVL system and treated in a developer to form a patterned photoresist coating. After an oxygen etching process of the graphene coating in the RIE system and the dissolution of the residual photoresist in acetone, the striated pattern was transferred from the photoresist to the graphene coating.

Electrochemical test

The tested electrodes were all assembled in Swagelok-type batteries in a glovebox filled with argon. The counter electrode was lithium metal, and the electrolyte used was 1 mol L^{-1} $LiPF_6$ solution with EC and DMC as the solvents. The assembled batteries were galvanostatically tested by using a battery tester (Land BA2100A, Wuhan LAND Electronics Co., Ltd), discharged to 100 μA h cm^{-2} and charged to 2.0 V *vs.* Li^+/Li at room temperature. The cyclic voltammetry (CV) test of the batteries was carried out through a multichannel potentiostat system (BioLogic VSP-300).

Physical characterization

The scanning electron microscopy (SEM) images and energy-dispersive X-ray spectra (EDX) of the electrodes were observed by using a Hitachi S-4800 SEM. Raman spectra were recorded by using a JY-T6400 Raman spectrometer using 532 nm wavelength laser light. The electrical conductivities of the electrodes were measured by using an Ecopia HMS-3000 Hall effect measurement system utilizing the four-probe method.

Results and discussion

The morphological characterization and component analysis of the as-prepared electrodes are presented in Fig. 2. Fig. 2a

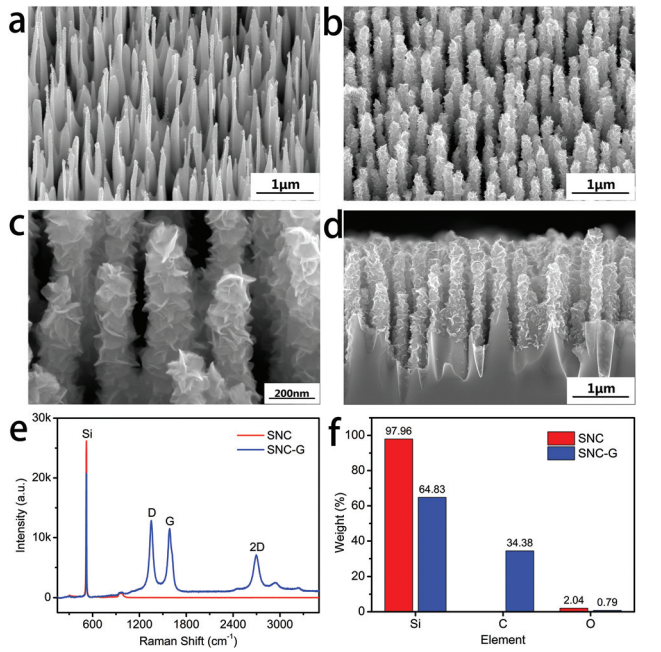

Fig. 2 (a) Tilted angle SEM image of the SNC electrode. (b) Tilted angle, (c) high-magnification tilted angle, and (d) cross-section SEM images of the SNC-G electrode. (e) Raman spectra and (f) EDX element weight ratios of the SNC electrode and the SNC-G electrode.

shows the tilted angle SEM image of the SNC electrode; Fig. 2b and d show the tilted angle and cross-section SEM images of the SNC-G electrode, respectively. Fig. 2c shows a high-magnification SEM image of the SNC-G electrode, which clearly shows that the graphene nanosheets are vertically grown on the silicon nanocones and look like petaloid clusters. The SNCs are vertically aligned with an average height of 2 μm and an average half-width of 100 nm, while the average half-width of the SNCs with vertical graphene coating is 200 nm. These nanocone structures have several advantages for demonstrating the exclusive influences of graphene coating on silicon anodes. First, the intercone space is sufficient for accommodating the volume expansion caused by silicon lithiation. Second, the nanocone structure is free of binders, conductive additives, current collectors, and substrate adhesion problems. Third, the regular cone shape is beneficial for observing the SEI formation on the electrodes. Under the influences of the internal stress and the external electric field, the graphene nanosheets grow vertically on the surface after covering the silicon nanocones, forming a three-dimensional petaloid structure.[27] Compared with general two-dimensional coating materials, the three-dimensional structure of the graphene coating is more beneficial for accommodating the strain of volume change during cycling, thus enhancing the mechanical integrity and improving the interfacial properties.[28] Moreover, the three-dimensional conductive network can better facilitate lithium transportation and promote the electronic conductivity of the SNC electrode.

Fig. 2e shows the Raman spectra of the SNC electrode and the SNC-G electrode. The peaks at 520 cm^{-1} are associated with the crystalline silicon, and the peaks marked as D, G, and 2D in the spectrum of the SNC-G electrode are the characteristic peaks of few-layer graphene.[25] Fig. 2f shows the EDX analysis of both the SNC electrode and the SNC-G electrode. The weight ratio of silicon in the SNC electrode is 97.96%, and the existence of a small amount of oxygen (2.04%) is ascribed to the surface oxidation. The SNC-G electrode contains silicon, carbon, and oxygen, of which the weight ratios are 64.83%, 34.38%, and 0.79%, respectively. In addition, the graphene coating significantly improves the electrical conductivity of the SNC electrode, which increases from 15.7 to 4.68×10^4 S m^{-1} according to the four-point probe measurement results.

The electrochemical performance of the SNC electrode and the SNC-G electrode at 1 C is presented in Fig. 3. The batteries are discharged to 100 μA h cm^{-2} (equivalent to 2200 mA h g^{-1} concerning the SNCs through estimation) and charged to 2.0 V *vs.* Li^+/Li, and the current density is set to 100 μA cm^{-2}. The discharge capacity is limited to a certain value to ensure that the lithiation occurs in the SNCs rather than in the silicon substrate. Fig. 3a and b show the cycling performance of the SNC electrode and the SNC-G electrode at 1 C. The initial charge capacities of the SNC electrode and the SNC-G electrode are 70.3 and 69.0 μA h cm^{-2}, respectively. After an activation process for a few cycles, the charge capacity of the SNC electrode is maintained at about 96.0 μA h cm^{-2} for 40 cycles and

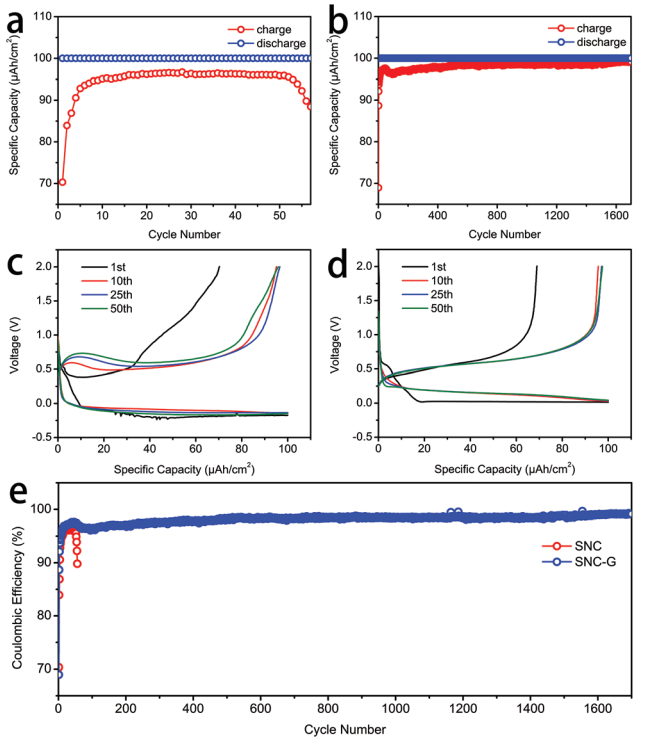

Fig. 3 Charge/discharge capacities of (a) the SNC electrode and (b) the SNC-G electrode at 1 C. The voltage profiles of (c) the SNC electrode and (d) the SNC-G electrode at 1 C for the 1st, 10th, 25th, and 50th cycles. (e) Coulombic efficiencies of the SNC electrode and the SNC-G electrode at 1 C.

fades rapidly afterwards. The charge capacity of the SNC-G electrode is maintained at about 98.5 μA h cm^{-2} for 1400 cycles and fades out after 1715 cycles. The reversible capacity and the cycle life of the SNC-G electrode are both superior to those of the SNC electrode.

Fig. 3c and d show the voltage profiles of the 1st, 10th, 25th, and 50th cycles of the SNC electrode and the SNC-G electrode, respectively. The charge plateau around 0.5 V is consistent with the behavior of silicon anodes.[29] The discharge voltage of the SNC electrode ends at −0.15 V, and the charge voltage starts at 0.5 V, indicating a high polarization of the SNC electrode. In this study, the cutoff condition of the discharging process is set to a fixed capacity rather than a certain voltage; thus, the lithiation process still continues even though the discharge voltage drops below 0 V as a non-equilibrium state due to polarization.[30,31] In the voltage profile of the SNC electrode, no charge/discharge plateau around 0 V is observed and the initial delithiation voltage (0.5 V) after the lithiation process is high above Li/Li^+, indicating that there is no lithium metal deposited onto the electrode and the polarization of the electrode is high. The discharge voltage of the SNC-G electrode ends at 0.04 V, and the charge voltage starts at 0.27 V, which indicates that the electrode polarization is improved by the graphene coating. In addition, the voltage profiles of the SNC-G electrode are highly similar for the 10th, 25th, and 50th cycles, indicating a stable electrochemical behavior.

Fig. 3e shows the Coulombic efficiencies of the SNC electrode and the SNC-G electrode. The initial Coulombic efficiency of the SNC-G electrode (69.0%) is slightly less than that of the SNC electrode (70.3%), which is associated with the initial SEI formation on the large specific surface area of the vertical graphene.[32] The SNC electrode fades out rapidly after 50 cycles with an average Coulombic efficiency of 94.6%, while the SNC-G electrode achieves 1715 cycles with an average Coulombic efficiency of 98.2%, indicating that the cycling stability and Coulombic efficiency of the SNC electrode are greatly enhanced by the graphene coating.

The graphene coating enhances the electrochemical performance of the SNC electrode in several ways. First, the graphene coating enhances the interfacial properties and protects the SNCs from coming into contact with the electrolyte directly; thus, the decomposition of the electrolyte and the related irreversible side reactions are suppressed, leading to higher reversible capacity and Coulombic efficiency of the electrode.[33] Second, the graphene coating helps to enhance the mechanical integrity of the SNCs, and the three-dimensional petaloid structure is more beneficial for accommodating the strain of volume change during cycling; therefore, the structural stability and cycle life of the electrode are greatly improved.[34] Third, the three-dimensional conductive network of vertical graphene can facilitate lithium transportation and promote electronic conductivity, resulting in better rate capability and lower electrode polarization of the electrode.[35] Nevertheless, it is also notable that the Coulombic efficiency of the SNC-G electrode is still insufficient for full lithium-ion batteries, which is associated with the SEI formation caused by the surface defects and functional groups as well as the large specific surface area of the vertical graphene.[36]

Further electrochemical characterization was also carried out to demonstrate the influences of graphene coating on silicon anodes. Fig. 4a and b show the CV curves of the SNC electrode and SNC-G electrode, respectively, with a scan rate of 0.1 mV s^{-1}. The broad cathodic peak at around 0.7 V is associated with the SEI formation on the electrode,[37] which disappears after the first cycle of the SNC-G electrode, yet exists for all the three cycles of the SNC electrode, indicating that the SEI formation of the SNC-G electrode is less than that of the SNC electrode. The cathodic peaks at around 0.2 V are attributed to the formation of amorphous Li_xSi alloys during the lithiation process.[38] Two anodic peaks at around 0.35 and 0.53 V of both the electrodes are the characteristic anodic peaks of the silicon anodes, which can be ascribed to the phase transition between amorphous Li_xSi and amorphous silicon.[39] In addition, the peak current of the SNC-G electrode is much larger than that of the SNC electrode, indicating that the higher electrical conductivity is attributed to graphene coating.

Fig. 4c shows the rate capabilities of the SNC-G electrode and SNC electrode. The cutoff conditions are discharging to 100 μA h cm^{-2} and charging to 2.0 V; and the current density varies from 20 to 500 μA cm^{-2} (0.2, 0.5, 1, 2, and 5 C). The reversible capacities of the SNC-G electrode are larger than those of the SNC electrode at different rates, indicating the superior rate capability of the SNC-G electrode, which can be associated with the higher electrical conductivity and thinner SEI layer attributed to graphene coating.[26] As shown in Fig. 4d, the cycling performance of the SNC-G electrode at 0.5 C is also tested. The cycle life of the SNC-G electrode (1678 cycles) is much longer than that of the SNC electrode (85 cycles), while the average Coulombic efficiency (96.0%) is still not high enough. This result is consistent with the situation at 1 C.

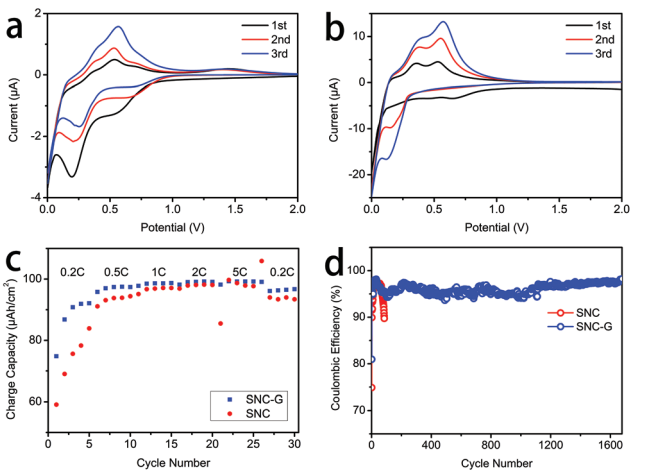

Fig. 4 Cyclic voltammogram curves of (a) the SNC electrode and (b) the SNC-G electrode for the 1st, 2nd, and 3rd cycles at 0.1 mV s^{-1}. (c) Rate capabilities of the SNC electrode and the SNC-G electrode at 0.2, 0.5, 1, 2, and 5 C. (d) Coulombic efficiencies of the SNC electrode and the SNC-G electrode at 0.5 C.

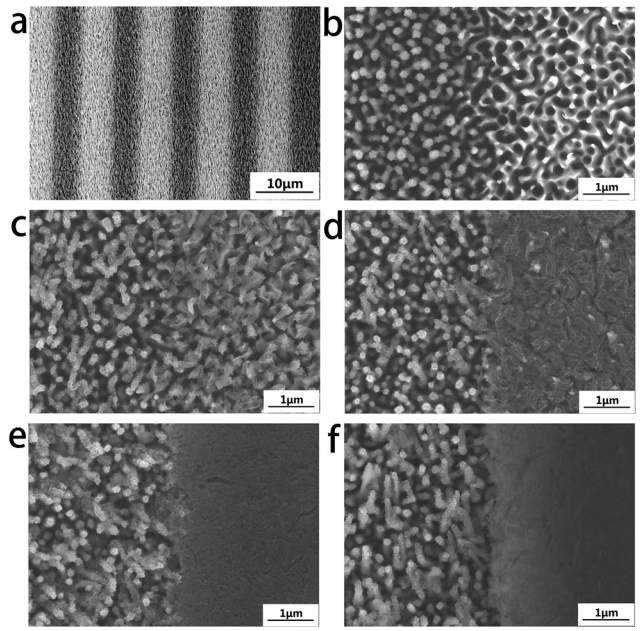

Fig. 5 (a) A low-magnification SEM image of the original SNC-PG electrode. The SEM images of the SNC-PG electrodes after (b) 0, (c) 10, (d) 25, (e) 50, and (f) 100 cycles, in which the left halves are the SNC-G area and the right halves are the SNC area.

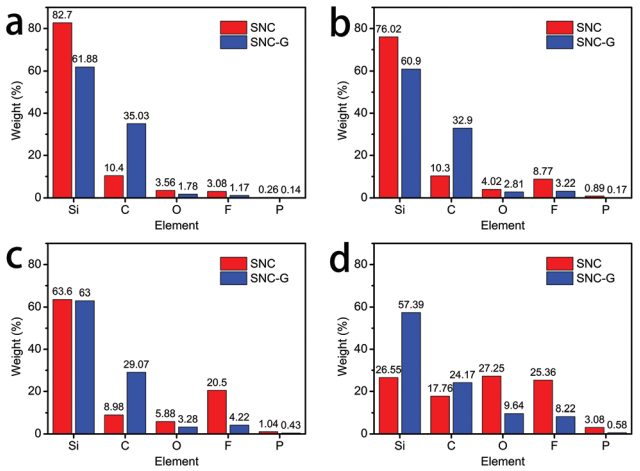

Fig. 6 EDX element weight ratios of the SNC area and the SNC-G area of the SNC-PG electrodes after (a) 10, (b) 25, (c) 50, and (d) 100 cycles.

To demonstrate the significant influences of graphene coating on the SEI formation and structural stability of silicon anodes, morphological and elemental analyses of the SNC-PG electrodes after different cycles were carried out by SEM and EDX. UVL and RIE technologies were applied to the SNC-G electrode to obtain the SNC-PG electrode. With this patterned electrode, the area with graphene coating (SNC-G area) and the area without graphene coating (SNC area) can be tested under exactly the same conditions, which makes the comparison between these two structures more direct and convincing. The discharge capacity is set to 100 μA h cm^{-2} and the current density is 50 μA cm^{-2}. Fig. 5a shows the original morphology of the SNC-PG electrode, in which the dark area is the SNC-G area and the bright area is the SNC area. Fig. 5b, c, d, e, and f show the SNC-PG electrodes after 0, 10, 25, 50, and 100 cycles, respectively, in which the left halves are the SNC-G area and the right halves are the SNC area. With the increase of cycle number, the SEI particles form on the SNC surface, aggregate into clusters, fill the intercone space, and eventually cover the SNC area. Meanwhile, the structure of the SNCs is severely damaged to a disordered state. As a comparison, the SEI formation on the SNC-G area is much less and more stable, and the SNC-G structure retains its original shape after 100 cycles, which are attributed to the high electrical conductivity, excellent chemical stability, and remarkable mechanical strength of the graphene coating.[24] The improvements of SEI formation and structural stability are consistent with the electrochemical performance of the SNC-G electrode.

Fig. 6a, b, c, and d show the corresponding EDX element weight ratios of the SNC-PG electrodes after 10, 25, 50, and 100 cycles, respectively. The element weight ratios of Si, C, O, F, and P are detected for both the SNC area and the SNC-G area. The increments of O, F, and P compared to the original electrode are ascribed to the formation of the SEI layer.[40] The comparison of the C element between the SNC area and the SNC-G area is not considered because of the existence of graphene coating. After 10 cycles, the weight ratios of O, F, and P of the SNC area are 3.56%, 3.08%, and 0.26%, respectively; the weight ratios of O, F, and P of the SNC-G area are 1.78%, 1.17%, and 0.14%, respectively. After 25 cycles, the weight ratios of O, F, and P of the SNC area are 4.02%, 8.77%, and 0.89%, respectively; the weight ratios of O, F, and P of the SNC-G area are 2.81%, 3.22%, and 0.17%, respectively. After 50 cycles, the weight ratios of O, F, and P of the SNC area are 5.88%, 20.5%, and 1.04%, respectively; the weight ratios of O, F, and P of the SNC-G area are 3.28%, 4.22%, and 0.43%, respectively. After 100 cycles, the weight ratios of O, F, and P of the SNC area are 27.25%, 25.36%, and 3.08%, respectively; the weight ratios of O, F, and P of the SNC-G area are 9.64%, 8.22%, and 0.58%, respectively. It can be concluded that the amount of SEI increases for both the SNC area and the SNC-G area as the cycle number increases, but the amount of SEI of the SNC-G area is always less than that of the SNC area. The elemental analysis is consistent with the SEM images in Fig. 5. Both the morphological and elemental analyses of the SNC-PG electrodes after different cycles indicate that the graphene coating has significant effects on maintaining the thin SEI layer and stable nanostructure of the silicon anodes; therefore, the Coulombic efficiency, the rate capability, and especially the cycle life of the SNC-G electrode get remarkably enhanced.

Conclusions

In conclusion, we have demonstrated the significant influences of the vertical graphene coating on the electrochemical performance, SEI formation, and structural stability of the

silicon anodes by the combined utilization of the SNC model anode and the coating patterning technology. The nanocone construction has the advantages of sufficient intercone space, pure components, and regular morphology. The patterning of graphene coating makes the comparison between the SNC structure and the SNC-G structure more direct and convincing. The SNC-G electrode shows a longer cycle life (1715 cycles), higher Coulombic efficiency (average 98.2%), better rate capability, and lower electrode polarization than the SNC electrode. On the SNC-PG electrode, the SNC-G area maintains a thin SEI layer and stable nanostructure during cycling, while the SNC area without graphene coating is gradually damaged and filled with SEI particles, and finally covered with a thick SEI layer after 100 cycles. Moreover, the combination of the nanocone structure and patterning technology can also be applied to other fundamental research studies of silicon anodes and coating materials for lithium-ion batteries.

Conflicts of interest

There are no conflicts of interest to declare.

Acknowledgements

The authors acknowledge the financial support from the Ministry of Science and Technology of China (Grant No. 2016YFA0200800 and 2016YFA0200400), the National Key R&D Program of China (Grant No. 2016YFB0100500 and 2016YFB0100100), the National Natural Science Foundation of China (Grant No. 91323304, 61390503, 11674387, 11574369, 11574385, 11574368, 52315206, and 51502334) and the "Strategic Priority Research Program" of the Chinese Academy of Sciences (Grant No. XDB07020200 and XDA09010000).

References

1 K. Kang, Y. S. Meng, J. Bréger, C. P. Grey and G. Ceder, *Science*, 2006, **311**, 977–980.
2 M. Armand and J.-M. Tarascon, *Nature*, 2008, **451**, 652–657.
3 W.-J. Zhang, *J. Power Sources*, 2011, **196**, 13–24.
4 H. Li, L. Shi, Q. Wang, L. Chen and X. Huang, *Solid State Ionics*, 2002, **148**, 247–258.
5 F. Luo, B. Liu, J. Zheng, G. Chu, K. Zhong, H. Li, X. Huang and L. Chen, *J. Electrochem. Soc.*, 2015, **162**, A2509–A2528.
6 N. Liu, H. Wu, M. T. McDowell, Y. Yao, C. Wang and Y. Cui, *Nano Lett.*, 2012, **12**, 3315–3321.
7 Y. Wang, Y. Liu, J. Zheng, H. Zheng, Z. Mei, X. Du and H. Li, *Nanotechnology*, 2013, **24**, 424011.
8 X. Li, M. Gu, S. Hu, R. Kennard, P. Yan, X. Chen, C. Wang, M. J. Sailor, J.-G. Zhang and J. Liu, *Nat. Commun.*, 2014, **5**, 4105.
9 C. K. Chan, H. Peng, G. Liu, K. McIlwrath, X. F. Zhang, R. A. Huggins and Y. Cui, *Nat. Nanotechnol.*, 2008, **3**, 31–35.
10 M. Ge, J. Rong, X. Fang and C. Zhou, *Nano Lett.*, 2012, **12**, 2318–2323.
11 H. Wu, G. Chan, J. W. Choi, I. Ryu, Y. Yao, M. T. McDowell, S. W. Lee, A. Jackson, Y. Yang, L. Hu and Y. Cui, *Nat. Nanotechnol.*, 2012, **7**, 310–315.
12 M.-H. Park, M. G. Kim, J. Joo, K. Kim, J. Kim, S. Ahn, Y. Cui and J. Cho, *Nano Lett.*, 2009, **9**, 3844–3847.
13 Y.-M. Lin, K. C. Klavetter, P. R. Abel, N. C. Davy, J. L. Snider, A. Heller and C. B. Mullins, *Chem. Commun.*, 2012, **48**, 7268–7270.
14 M. H. Ryou, J. Kim, I. Lee, S. Kim, Y. K. Jeong, S. Hong, J. H. Ryu, T. S. Kim, J. K. Park and H. Lee, *Adv. Mater.*, 2013, **25**, 1571–1576.
15 J. R. Szczech and S. Jin, *Energy Environ. Sci.*, 2011, **4**, 56–72.
16 N. Dimov, S. Kugino and M. Yoshio, *Electrochim. Acta*, 2003, **48**, 1579–1587.
17 X. Zhou, Y.-X. Yin, A.-M. Cao, L.-J. Wan and Y.-G. Guo, *ACS Appl. Mater. Interfaces*, 2012, **4**, 2824–2828.
18 H. Xiang, K. Zhang, G. Ji, J. Y. Lee, C. Zou, X. Chen and J. Wu, *Carbon*, 2011, **49**, 1787–1796.
19 Y. Yu, L. Gu, C. Zhu, S. Tsukimoto, P. A. van Aken and J. Maier, *Adv. Mater.*, 2010, **22**, 2247–2250.
20 Y. He, X. Yu, Y. Wang, H. Li and X. Huang, *Adv. Mater.*, 2011, **23**, 4938–4941.
21 Y. Shi, L. Wen, G. Zhou, J. Chen, S. Pei, K. Huang, H.-M. Cheng and F. Li, *2D Mater.*, 2015, **2**, 024004.
22 J. Xu, I.-Y. Jeon, H.-J. Choi, S.-J. Kim, S.-H. Shin, N. Park, L. Dai and J.-B. Baek, *2D Mater.*, 2016, **4**, 014002.
23 X. Zhou, Y.-X. Yin, L.-J. Wan and Y.-G. Guo, *Chem. Commun.*, 2012, **48**, 2198–2200.
24 R. Hu, W. Sun, Y. Chen, M. Zeng and M. Zhu, *J. Mater. Chem. A*, 2014, **2**, 9118–9125.
25 C. Wang, Y.-S. Chui, R. Ma, T. Wong, J.-G. Ren, Q.-H. Wu, X. Chen and W. Zhang, *J. Mater. Chem. A*, 2013, **1**, 10092–10098.
26 X. Zhou, Y. X. Yin, L. J. Wan and Y. G. Guo, *Adv. Energy Mater.*, 2012, **2**, 1086–1090.
27 L. Li, W. Sun, S. Tian, X. Xia, J. Li and C. Gu, *Nanoscale*, 2012, **4**, 6383–6388.
28 C. Wang, Y. Li, Y.-S. Chui, Q.-H. Wu, X. Chen and W. Zhang, *Nanoscale*, 2013, **5**, 10599–10604.
29 F. M. Hassan, A. R. Elsayed, V. Chabot, R. Batmaz, X. Xiao and Z. Chen, *ACS Appl. Mater. Interfaces*, 2014, **6**, 13757–13764.
30 F. Luo, G. Chu, X. Xia, B. Liu, J. Zheng, J. Li, H. Li, C. Gu and L. Chen, *Nanoscale*, 2015, **7**, 7651–7658.
31 C. Wang, F. Luo, H. Lu, X. Rong, B. Liu, G. Chu, Y. Sun, B. Quan, J. Zheng, J. Li, C. Gu, X. Qiu, H. Li and L. Chen, *ACS Appl. Mater. Interfaces*, 2017, **9**, 2806–2814.
32 H. Kim, D.-H. Seo, S.-W. Kim, J. Kim and K. Kang, *Carbon*, 2011, **49**, 326–332.
33 X. Su, Q. Wu, J. Li, X. Xiao, A. Lott, W. Lu, B. W. Sheldon and J. Wu, *Adv. Energy Mater.*, 2014, **4**, 1300882.
34 I. H. Son, J. H. Park, S. Kwon, S. Park, M. H. Rümmeli, A. Bachmatiuk, H. J. Song, J. Ku, J. W. Choi and J.-M. Choi, *Nat. Commun.*, 2015, **6**, 8597.

35 W. Zhang, P. Zuo, C. Chen, Y. Ma, X. Cheng, C. Du, Y. Gao and G. Yin, *J. Power Sources*, 2016, **312**, 216–222.
36 D. Pan, S. Wang, B. Zhao, M. Wu, H. Zhang, Y. Wang and Z. Jiao, *Chem. Mater.*, 2009, **21**, 3136–3142.
37 Y. Xu, G. Yin, Y. Ma, P. Zuo and X. Cheng, *J. Mater. Chem.*, 2010, **20**, 3216–3220.
38 K. Evanoff, A. Magasinski, J. Yang and G. Yushin, *Adv. Energy Mater.*, 2011, **1**, 495–498.
39 B. Wang, X. Li, X. Zhang, B. Luo, M. Jin, M. Liang, S. A. Dayeh, S. Picraux and L. Zhi, *ACS Nano*, 2013, **7**, 1437–1445.
40 A. L. Michan, G. Divitini, A. J. Pell, M. Leskes, C. Ducati and C. P. Grey, *J. Am. Chem. Soc.*, 2016, **138**, 7918–7931.